ACS APPLIED POLYMER MATERIALS

pubs.acs.org/acsapm Article

Increasing Ductility and Toughness of Photocurable Thermosets with Microstructures Controlled by Phase Separation

Lauren Zakrzewski, Kanta Das Purkaysta, Chulsung Bae, and Catalin R. Picu*

Cite This: ACS Appl. Polym. Mater. 2024, 6, 5028−5038 Read Online

ACCESS | Metrics & More | Article Recommendations | Supporting Information

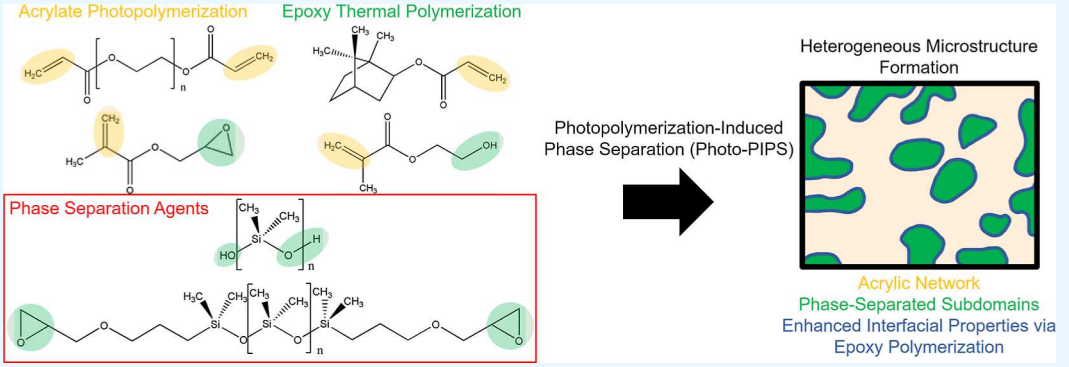

ABSTRACT: In this work, photopolymerization-induced phase separation (photo-PIPS) is implemented into a polymer network consisting of both acrylic and epoxy-based chemistries to allow for the development of an acrylic network through photopolymerization and for enhanced strength and stiffness to be obtained via thermal cross-linking of the epoxy-based chemistries. Two epoxy-based end-group terminated polydimethylsiloxane (PDMS) polymer additives [hydroxy-terminated PDMS (OH-PDMS) and diglycidyl ether-terminated PDMS (epoxy-PDMS)] are added to enable phase separation, creating a heterogeneous polymeric material. During thermal treatment applied after photopolymerization, these additives can cross link together, concurrently with the cross-linking of the epoxy-based monomers which are part of the network, therefore creating elastomeric, phase-separated subdomains. Mixtures of OH-PDMS and epoxy-PDMS of various molar ratios are used to alter the extent of phase separation and the amount of cross-linking that occurs within the subdomains. It is observed that OH-PDMS does not phase separate when present alone, while it separates in the presence of epoxy-PDMS. Cross-linking within the phase-separated domains containing both types of PDMS leads to enhanced ductility, with the optimal ductility and toughness enhancement being obtained for the PDMS stoichiometry (OH-PDMS:epoxy-PDMS 80:20 by mol %). This composition retains good creep resistance and has only a slightly smaller strength than the neat resin.

KEYWORDS: *photo-PIPS, phase separation, thermosets, kinetics, thermal cross-linking*

1. INTRODUCTION

The development of diverse thermosetting network architectures is of great interest in the field of materials science. Vast potential applications exist for heterogeneous thermosets including polymer dispersed liquid crystals,[1−5] polymer membranes,[6−9] polymer composites,[10−12] and applications enabled by stereolithography (SLA) 3D printing.[13−15]

Various techniques have been developed to create heterogeneous polymeric materials including polymer blends,[16−22] block copolymer self-assembly,[23−26] the addition of elastomeric particles and of nanoparticles,[27−37] and polymerization-induced phase separation (PIPS).[1,31,38−50] All of these methods have their own advantages and disadvantages, such as the cost and strict processing conditions. However, among them, PIPS offers unique opportunities such as the development of various microstructures, including droplet-like or interpenetrating subdomains, obtained by a simple variation of the chemical composition and/or light intensity used for photopolymerization. Due to this, PIPS is used in this study.

PIPS begins with an initially homogeneous liquid photocurable mixture consisting of monomers, which polymerize into a thermosetting network, and a phase-separating agent, which phase-separates upon polymerization.[1,39,40,42−46] This process can be initiated through several reactive pathways such as anionic, cationic, thermal, or radical-light-initiated polymer-

Received: December 23, 2023
Revised: February 28, 2024
Accepted: April 4, 2024
Published: April 18, 2024

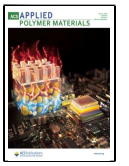

https://doi.org/10.1021/acsapm.3c03155
ACS Appl. Polym. Mater. 2024, 6, 5028−5038

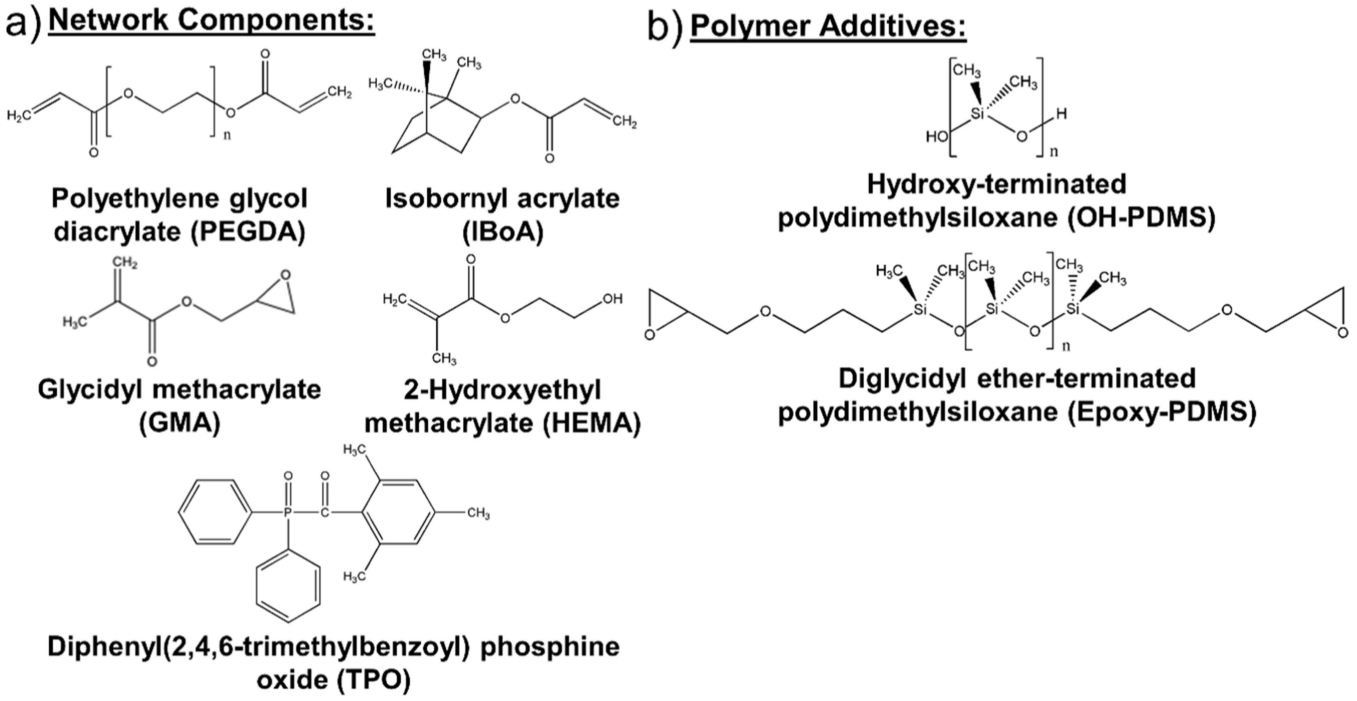

Figure 1. (a) Structure of the photopolymerizing network components including monomers and photoinitiator and (b) polymer additives used for phase separation.

ization (photo-PIPS). Among these polymerization processes, photo-PIPS was selected for this work due to the ease of controlling the polymerization kinetics.

Several challenges have been identified when using photo-PIPS: (i) the interfacial properties between the network and phase-separated subdomains need to be controlled, (ii) the morphology and dimensions of the phase-separated subdomains are often only indirectly controlled, and (iii) internal stress can develop during the photopolymerization process.[31,51] Controlling the interfacial properties is important, as poor adhesion weakens load transfer between the network and subdomains, which typically reduces the strength and stiffness of the material. The interface strength can be controlled using block copolymers, or by bonding the material within the phase-separated subdomains to the network after photopolymerization and phase separation.[31,52,53] The sizes and shapes of these subdomains can be altered by varying the phase-separating agent's molecular weight, concentration and/or chemistry, and by adjusting the photopolymerization kinetics.[40,42,45,46] Internal stresses may develop during curing and network shrinkage and can cause early failure of materials. Controlling the polymerization kinetics and the extent of monomer conversion can help minimize the stress and reduce the extent of network shrinkage during polymerization.[54−62]

Alterations of the monomer chemistries within the initially homogeneous resin, such as variation of the reactive end-group chemistry, can have effects on the network and the resulting material properties. Using acrylic or epoxy-based monomers, different reactive pathways exist; acrylics typically react via photopolymerization,[63−65] and epoxies react via chain-growth ring-opening polymerization or step-growth polymerization.[66−68] Combining the various chemistries of epoxies and acrylics into one photo-PIPS resin may allow for further control of the microstructure and material properties.

While various solutions to improve the ductility and toughness of acrylic- and epoxy-based thermosets exist, including the use of elastomeric microbeads, copolymers, and nanoparticles, little attention has been given to a phase-separation-based approach for the same purpose. In our previous study,[46] we explored the mechanical properties of several photocurable resins in which phase separation of polypropylene glycol (PPG) occurs. This work indicated that PPG works both as a plasticizer and as a phase-separating agent and that the plasticizing effect may be dominant. Furthermore, it was observed that the state of the subdomains is critical, with a drastic reduction of properties resulting if the additive is in the liquid state at room/testing temperature. A solution to this is to use an additive that is in the solid state at room temperature and to perform polymerization at an elevated temperature to temporarily melt the polymer additive, enabling diffusion and phase separation. Another solution, which is explored in this work, is to allow phase separation to occur under ambient conditions and later cross-link the polymer additive after the subdomains are formed.

Thus, this work focuses on the development of a network composed of both acrylic- and epoxy-based monomers, allowing for photopolymerization of the acrylic-based end-groups to develop the network and, in a subsequent processing step, for the thermal cross-linking of the epoxy-based end-groups to enhance the material stiffness and strength. Furthermore, linear polymer chains of PDMS with epoxy-based end-groups are used as the phase-separating agents. Phase separation takes place during photopolymerization. The PDMS chains within the phase-separated subdomains cross link with each other during the thermal processing step. This, in turn, yields an enhanced ductility and toughness of the bulk material. The epoxy-based end-groups of PDMS are also expected to be able to cross-link with epoxy-based end-groups

https://doi.org/10.1021/acsapm.3c03155
ACS Appl. Polym. Mater. 2024, 6, 5028−5038

present within the network, enhancing subdomain-network interfacial properties.

2. MATERIALS AND METHODS

2.1. Materials. A diacrylate oligomer, polyethylene glycol diacrylate (PEGDA, M_n = 575 g/mol), an acrylate diluent, isobornyl acrylate (IBoA, M_n = 208 g/mol), two methacrylate diluents, glycidyl methacrylate (GMA, M_n = 142 g/mol), and 2-hydroxyethyl methacrylate (HEMA, M_n = 130 g/mol), and a photoinitiator, diphenyl(2,4,6-trimethylbenzoyl) phosphine oxide (TPO, M_n = 348 g/mol), are used for the development of the photopolymerized acrylic network. Additionally, the methacrylate diluents are specifically used to enable thermal cross-linking of their epoxide and alcohol chemistries after photopolymerization of the acrylic chemistries. Figure 1a portrays the chemical structures of the various components used to develop the photopolymerized acrylic network.

Various polymer additives are considered for the implementation of phase separation, including hydroxy-terminated polydimethylsiloxane (OH-PDMS, M_n = 550 g/mol) and diglycidyl ether-terminated polydimethylsiloxane (epoxy-PDMS, M_n = 800 g/mol). The two polydimethylsiloxane polymer additives are used in conjunction with one another to allow for thermal cross-linking within the phase-separated subdomains. Figure 1b depicts the chemical structures of the polymer additives considered. All chemicals used are purchased from Sigma-Aldrich.

The neat resin consists of a molar ratio of 15:85 PEGDA/IBoA with an additional 20 mol % of GMA and 20 mol % of HEMA (15:85:20:20 PEGDA/IBoA:GMA/HEMA or 11:61:14:14 PEGDA/IBoA:GMA/HEMA). To this mixture, 0.3 mol % of TPO photoinitiator is added and dissolved in powder form with stirring and gentle heating to ∼60 °C to create the photocurable neat resin, denoted as "PIGH20" for "**P**EGDA/**I**BoA:**G**MA/**H**EMA" with "20" standing for the mole percent of GMA and HEMA.

Phase-separating resins which contain OH-PDMS and epoxy-PDMS consist of 10 wt % of total polymer additive, which is dissolved into the PIGH20 neat resin with stirring and gentle heating to ∼60 °C. Various molar ratios of OH-PDMS to epoxy-PDMS within the PDMS-containing resins are considered: 0:100, 20:80, 40:60, 60:40, 80:20, 90:10, and 100:0. These stoichiometries are considered to not only alter the amount of cross-linking capable during the thermal cross-linking step but also alter the amount of phase separation present in the material, as discussed in Section 3. The notation for these resins is "PIGH20 OH-PDMS:epoxy-PDMS," (e.g., PIGH20 0:100, PIGH20 20:80, etc.). Seven different phase-separating resins based on PDMS are created and characterized.

2.2. Material Characterization. A custom-built light transmission apparatus previously described and employed in our previous studies[45,46,69] is used to evaluate the extent of phase separation in the photocurable resins. Transmittance tests are performed using a film thickness, b, of 100 μm, which is controlled using Scotch tape placed on a glass slide as a spacer. Liquid resin is added to the glass slide prepped with spacers; a coverslip is placed on top, and the sample is placed in the light transmission apparatus and irradiated with light of wavelength 405 nm and of intensity 5.2 mW/cm^2 for 15 min with transmission data collection occurring every 30 ms.

Resin samples developing phase separation exhibit a reduction in light transmission due to light scattering caused by the different refractive indices (RI) of the developing network and the phase-separated subdomains. The scattering is likely due to a combination of both Rayleigh and Mie scattering since the phase-separated subdomains likely have a large size distribution, with dimensions on the order of tens of nanometers, as well as larger than the wavelength of light used for irradiation (405 nm), respectively.[70] The induction time of phase separation is defined as the time at which such a reduction in transmittance occurs. After the initial reduction, transmittance increases again due to the mechanisms discussed in our previous study[45] (i.e., TPO consumption and microstructural refinement).

Real-time FTIR spectroscopy is performed during photopolymerization using a Thermo-Scientific Nicolet iS50 FT-IR equipped with an attenuated total reflectance (ATR) attachment (PIKE Technologies GladiATR) to determine various factors, including monomer conversion, induction time of photopolymerization, and rate of photopolymerization of the various resins. A LX500 OmniCure portable LED UV lamp of wavelength 405 nm is used for photopolymerization. A wavenumber range of 4000 to 400 cm^{-1} is used during photopolymerization. Scotch tape is added to the ATR stage to maintain a sample thickness of 100 μm; a drop of liquid resin is added to the ATR crystal, and a coverslip is placed on top. A custom-made 3D-printed part is used to hold the LED UV lamp and cover the stage. This part is positioned over the top of the resin sample, and photopolymerization occurs for a duration of 30 min with data collection occurring every 0.08 s. The light intensity is consistently held at 5.2 mW/cm^2.

Monomer conversion is obtained by comparing the peak heights of the (meth)acrylate carbonyl −C═O stretching peak at 1724 cm^{-1} and the (meth)acrylate alkene −C═C stretching peak at 1635 cm^{-1}. Within the Omnic software, these ratios in units of absorbance, A, are then used to calculate the conversion with respect to time using the equation

$$C(t)[\%] = (1 - A(t)/A(0)) \times 100 \quad (1)$$

From the monomer conversion curves, the induction time of photopolymerization can be obtained and is defined as the time at which monomer conversion begins to increase from 0%. Additionally, taking the derivative of the monomer conversion curve results in a rate of photopolymerization with respect to time.

Polymer film morphologies are examined using a Versa 3-D focused ion beam − scanning electron microscope by Thermo Fisher Scientific. Polymer films of 100 μm thickness are prepared in the same manner as for light transmittance experiments—with a duration of light irradiation of 15 min and a light intensity of 5.2 mW/cm^2. Films are then removed from the glass slide and coverslip, patted dry of residual resin, and placed in a bath of liquid nitrogen for 30 s. These are then fractured with a razor and washed for 2 min with ethyl ether to remove the phase-separated PDMS polymer additive. Films are then placed on an SEM stub, sputter coated with a layer of Au/Pd, and imaged using an accelerating voltage of 5.0 kV, a working distance of 10 mm, and a beam current of 5.9 pA. MATLAB is used to calculate the coefficient of variation (CV) of the grayscale of the SEM images to acquire a unitless measurement of roughness. CV is the ratio of the standard deviation to the mean of the pixel-by-pixel SEM image intensity.

Differential scanning calorimetry (DSC) Q2000 instrument from TA Instruments is used for running DSC on various resins to detect the temperature of thermally activated polymerization. For sample preparations, approximately 5−20 mg of solid photopolymerized sample is placed into a DSC pan, which is sealed with a lid. During experimentation, a temperature range of 30 to 225 °C is used with a temperature ramp of 10 °C/min. Photopolymerized samples are created using a light intensity of 5.2 mW/cm^2 and a duration of 30 min.

Dynamic mechanical analysis (DMA) is performed with a TA Instruments Discovery DMA 850. Samples with dimensions 40 × 12 × 3.2 mm^3 are used. Samples are prepared with custom-made silicone molds, a glass plate to cover the top and ensure planarity, and the UVO-Cleaner as previously described to irradiate with light of a wavelength of 405 nm for 30 min at 5.2 mW/cm^2 light intensity. DMA is performed with a temperature range of −150 to 150 °C and a temperature ramp of 3 °C/min. Liquid nitrogen and a TA Instruments gas cooling accessory (GCA) are used to achieve low temperatures. DMA tests are performed using the single cantilever method in bending mode with an oscillation amplitude of 5 μm, a frequency of 1 Hz, and an initial preload force of 0.01 N.

Molded polymer materials are subjected to tension using an Instron 5943 instrument equipped with a 1 kN load cell. Tensile dogbone specimens of dimensions 26 × 3.2 × 1.8 mm gauge length by width by thickness are prepared using custom-made silicone molds, a glass plate

https://doi.org/10.1021/acsapm.3c03155
ACS Appl. Polym. Mater. 2024, 6, 5028−5038

to cover the top and ensure planarity, and a UVO-Cleaner 342 from Jelight Companies, Inc. to irradiate for 30 min with light of 405 nm wavelength and 5.2 mW/cm^2 intensity. The ASTM638 standard is followed for tensile tests with dogbone specimens subjected to a strain rate of 6.4×10^{-3} s^{-1} at room temperature. Young's modulus from the tensile experiment is calculated by obtaining the slope of the stress−strain curve in the range of strains 0 to 1%.

Creep experiments are performed using the same dogbone specimen dimensions. Samples are subjected to constant stress at room temperature. The applied stress is varied from sample to sample and is a percentage (10, 20, and 35%) of the given sample's respective peak stress as determined from the stress−strain curve measured in monotonic uniaxial tensile tests. All creep experiments are performed for 8000 s or until fracture.

3. RESULTS AND DISCUSSION

3.1. Phase Separation Detection and Photopolymerization Kinetics. To create elastomeric subdomains, we consider the use of PDMS-based phase-separating additives which can cross-link upon thermal curing. Specifically, two different end-group terminated PDMS polymer additives (OH-PDMS and epoxy-PDMS as defined in Section 2.1), are added with a total concentration of 10 wt % to the PIGH20 neat resin to enable thermal cross-linking of the polymer additives. In the PIGH20 system, OH-PDMS does not induce phase separation, while epoxy-PDMS does, as indicated by the light transmittance curves in Figure 2. Specifically, the curve of the resin

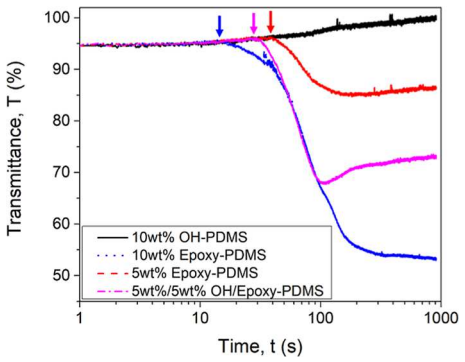

Figure 2. Light transmittance versus time curves for the PIGH20 PDMS-containing resins of various weight percent concentrations. Light irradiation begins at t = 0 s.

containing only OH-PDMS has no reduction in transmittance and increases over time, following the reactive Beer−Lambert law as mentioned in previous studies,[45,46] implying that the transmittance increases due to TPO photoinitiator consumption. When the two PDMS additives are mixed, the OH-PDMS also phase separates along with epoxy-PDMS because the two polymer additives possess the same polymer backbone, which enables the affinity of the PDMS molecules with each other. The 5/5 wt % OH/epoxy-PDMS curve of Figure 2 confirms this claim as the change in transmittance of this curve is larger than for 5 wt % epoxy-PDMS, indicating that more than 5 wt % of epoxy-PDMS has phase separated.

Therefore, the mixed systems of OH-PDMS and epoxy-PDMS phases separate simultaneously, which creates the premise for cross-linking within the subdomains to take place in a subsequent thermal curing step. However, to obtain the desired increase in material ductility by producing elastomeric-type properties within the subdomains, the degree of cross-linking within these subdomains needs to be controlled. Therefore, the relative molar ratio of OH-PDMS and epoxy-PDMS is varied to determine the optimal amount of cross-linking.

The light transmittance curves of Figure 3a correspond to various molar ratios of OH-PDMS/epoxy-PDMS. An expected trend of increasing extent of phase separation with increasing concentration of epoxy-PDMS and reducing concentration of OH-PDMS is seen. This effect is also shown in Figure 3b, where the change in transmittance is plotted with respect to the OH-PDMS concentration. In addition, a trend of increasing induction time of phase separation with increasing OH-PDMS concentration is shown in Figure 3c. This validates further that OH-PDMS is nonphase-separating and reduces the drive for phase separation when present in larger concentrations with epoxy-PDMS.

Real-time FTIR is performed on all these systems, and the corresponding monomer conversion curves are depicted in Figure 4. There is no particular trend in monomer conversion with increased extents of phase separation (i.e., increasing epoxy-PDMS content). Table 1 shows the relevant conversion data obtained from Figure 4, i.e., the maximum conversion reached within the exposure time considered, the induction time of photopolymerization, and the maximum rate of polymerization. A comparison of the photopolymerization induction times and the induction times of phase separation (Figure 3) indicates that phase separation occurs after the onset of photopolymerization in all PDMS-containing resins, and the delay becomes longer with increasing OH-PDMS content. This means that since OH-PDMS is nonphase-separating, increasing the OH-PDMS content reduces the phase separation kinetics.

The morphology of the PIGH20 neat and PDMS-containing resins after photopolymerization, before thermal cross-linking and after removal of PDMS, is studied by SEM and depicted in Figure 5. The PIGH20 neat resin exhibits no visible pores. However, large pores (subdomains) are visible in the PIGH20 0:100 system after washing with ethyl ether. With increasing concentration of OH-PDMS, the pores decrease in size and ultimately disappear in the PIGH20 100:0 resin due to the OH-PDMS being nonphase-separating. The CV of the gray level is computed for each of the images to provide a unitless measurement of the roughness of the observed surface. This provides a quantitative evaluation of the porosity and extent of phase separation of the corresponding resin systems (Figure 5). The PIGH20 neat resin and PIGH20 100:0 have comparable and low CVs (0.080 and 0.085, respectively), agreeing with the transmittance data, which indicates that phase separation is absent in these systems (Figure 3). The CVs for all the phase-separating resins are comparable and rather large (0.344 to 0.430 for PIGH20 0:100, 20:80, 40:60, and 60:40). The less phase-separating resins show a reduction in CV with a reducing extent of phase separation (CV = 0.301 for PIGH20 80:20 and CV = 0.206 for PIGH20 90:10). These SEM results confirm that the extent of phase separation in PIGH20 PDMS-containing resins is controlled by the amount of epoxy-PDMS present in the resin.

3.2. Thermal and Mechanical Properties of PDMS-Containing Resins. After photopolymerization, the resins are subjected to thermal curing by exposure to 165 °C for 48 h. The conditions for thermal curing are determined based on a separate study whose results are discussed in Figure S1 of the Supporting Information.

https://doi.org/10.1021/acsapm.3c03155
ACS Appl. Polym. Mater. 2024, 6, 5028−5038

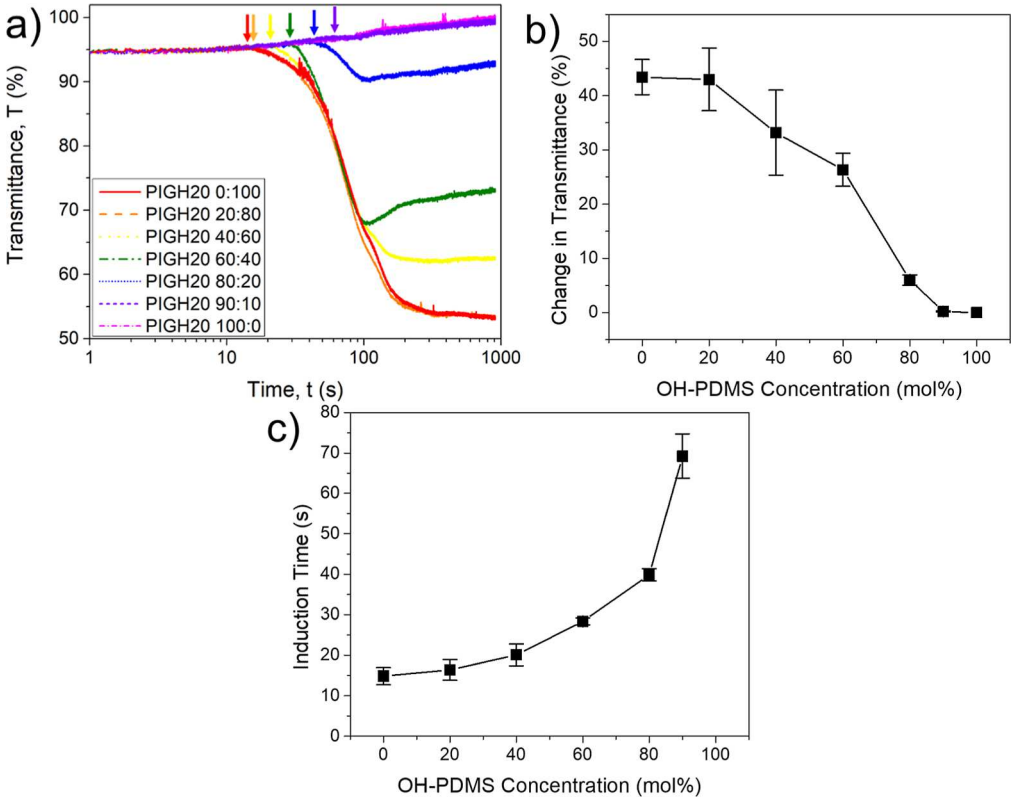

Figure 3. (a) Light transmittance versus time curves for the PIGH20 systems containing 10 wt % PDMS, with various molar ratios of OH-PDMS to epoxy-PDMS. Light irradiation begins at t = 0 s. Arrows indicate the induction time of phase separation (onset of the reduction in transmittance). (b) Change in transmittance and (c) respective induction times of phase separation. The change in transmittance reported is the difference in transmittance from the induction time to the minimum in the transmittance curves of (a). Error bars represent the 95% confidence interval of three replicates per sample.

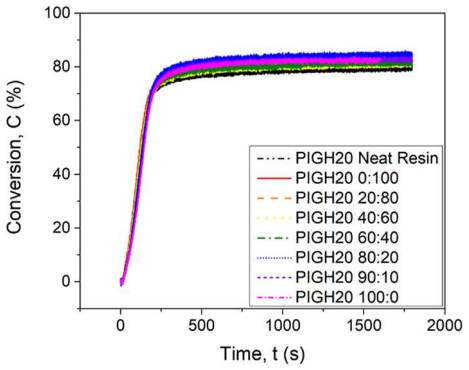

Figure 4. Monomer conversion curves of the PIGH20 neat and PDMS-containing resins obtained via real-time FTIR. Light irradiation begins at t = 0 s.

Table 1. Values of Monomer Conversion After 900 s of Exposure Time, Induction Time for Photopolymerization, and Maximum Rate of Polymerization for the PIGH20 Neat and PDMS-Containing Resins, as Obtained from Figure 4. The Reported Error Represents the Standard Error of Three Replicates

resin	conversion, C (%)	induction time (s)	maximum rate of polymerization, Rp (s−1)
PIGH20 neat resin	75.7 ± 3.6	10.03 ± 0.22	0.605 ± 0.013
PIGH20 0:100	81.7 ± 0.1	11.09 ± 0.39	0.600 ± 0.004
PIGH20 20:80	83.3 ± 0.6	11.36 ± 0.02	0.579 ± 0.007
PIGH20 40:60	81.9 ± 0.8	11.28 ± 0.20	0.585 ± 0.012
PIGH20 60:40	81.9 ± 0.4	11.11 ± 0.07	0.561 ± 0.008
PIGH20 80:20	83.4 ± 1.5	11.54 ± 0.08	0.543 ± 0.002
PIGH20 90:10	82.4 ± 0.5	9.70 ± 0.84	0.561 ± 0.011
PIGH20 100:0	83.0 ± 0.3	11.41 ± 0.05	0.568 ± 0.008

To verify whether thermal curing indeed enables cross-linking of the epoxy-based chemistries, DSC has been performed to visualize the temperature at which thermal polymerization is activated for both acrylate and epoxy-based chemistries. Figure 6a portrays the DSC curves of a resin comprising PEGDA/IBoA 15:85 by mol % with 0.3 mol % TPO and of the PIGH20 neat resin. Both samples are photopolymerized for 30 min at 5.2 mW/cm^2 light intensity prior to DSC testing as indicated in Section 2.2. It shows that a broad exothermic peak exists for the PIGH20 neat resin around 160−210 °C, while a narrower exothermic peak around 180−215 °C exists for the PEGDA/IBoA 15:85 resin. This indicates that acrylates do in fact polymerize via thermal activation at temperatures higher than 180 °C, as supported by the PEGDA/IBoA resin, which contains no amount of epoxy-based chemistries. However, the addition of the epoxy-based chemistries lowers this thermal activation temperature, as indicated by the PIGH20 neat resin curve of Figure 6a. The

https://doi.org/10.1021/acsapm.3c03155
ACS Appl. Polym. Mater. 2024, 6, 5028−5038

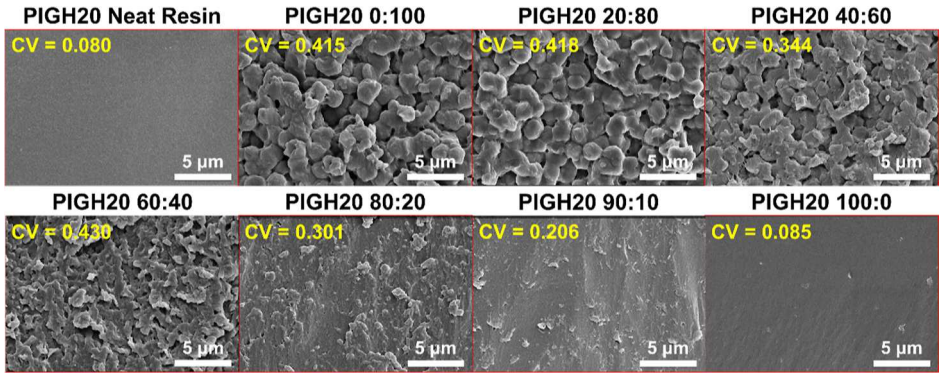

Figure 5. SEM images of the fractured cross sections of the PIGH20 neat and PDMS-containing polymer films as prepared using the parameters discussed in Section 2.2. A magnification of 10 000x is used for imaging. The CV of the gray level for each image is provided as a unitless measure of roughness and hence of phase separation.

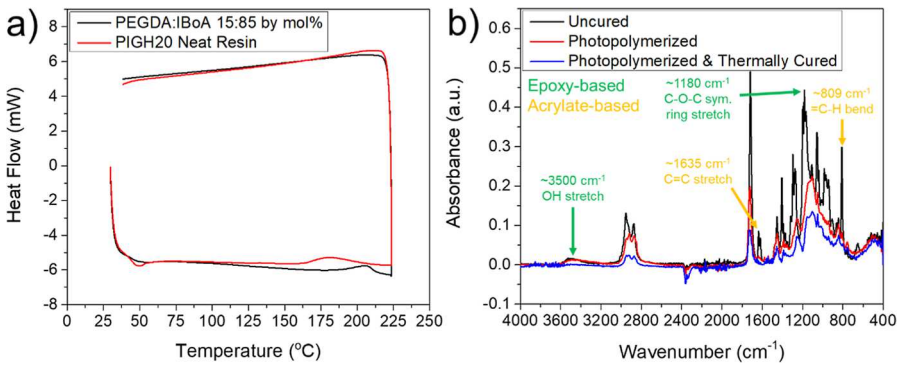

Figure 6. (a) DSC curves for the PIGH20 neat resin and a resin comprised of PEGDA/IBoA 15:85 by mol % with 0.3 mol % TPO photoinitiator. (b) FTIR spectra of the PIGH20 neat resin uncured, photopolymerized, and photopolymerized with additional thermal treatment. Photopolymerization was performed via light irradiation for 30 min at 5.2 mW/cm^2 light intensity, and thermal treatment was performed at 165 °C for 48 h.

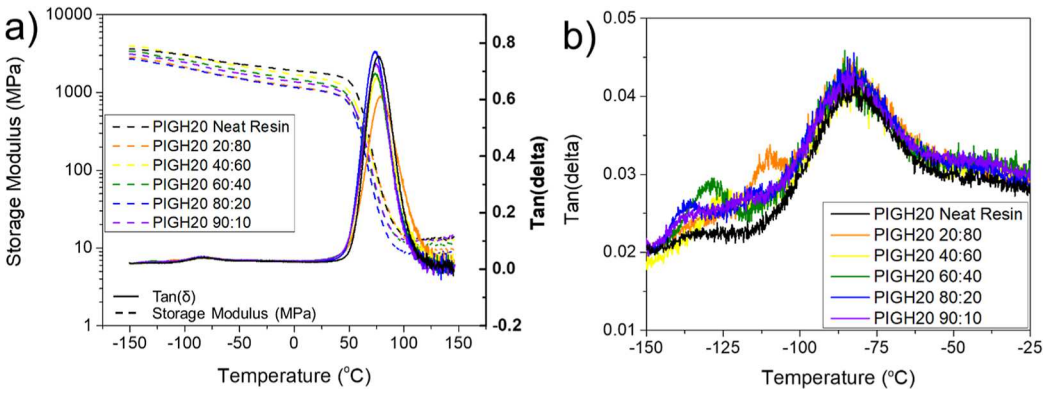

Figure 7. (a) The storage modulus and tan(δ) curves obtained by DMA analysis for the PIGH20 neat and PDMS-containing resins thermally cured at 165 °C for 48 h. (b) A zoomed view of the low-temperature region of the tan(δ) curves for easier visualization of the PDMS T_g. Two replicates are performed for each resin system.

thermal activation temperature exists as a broad peak, indicating that both acrylic and epoxy cross-linking occur between temperatures of 160 and 210 °C in the PIGH20 neat resin.

Further, FTIR probing is performed for the PIGH20 neat resin in the liquid uncured state, the photopolymerized state, and the photopolymerized and thermally treated state to support the findings from DSC. Figure 6b portrays these three samples' FTIR spectra and indicates that the acrylate peaks present at 1635 cm^{-1} (C═C stretch) and at 809 cm^{-1} (═C−H bend) diminish from the uncured state to the photopolymerized state, as expected. These peaks slightly reduce further from the photopolymerized state to the photopolymerized and thermally treated state, which is an indication that further acrylate polymerization occurs during thermal treatment. Additionally, epoxy cross-linking is confirmed to occur during thermal treatment due to the visible reduction of the OH stretch at ∼3500 cm^{-1} (present from HEMA), from the photopolymerized state to the photopolymerized and thermally treated state. Furthermore, the C−O−C "breathing"

https://doi.org/10.1021/acsapm.3c03155
ACS Appl. Polym. Mater. 2024, 6, 5028−5038

stretch at ∼1180 cm^{-1} (present from GMA) also reduces in the same manner. Interestingly, these two peaks slightly reduce from the uncured state to the photopolymerized state, indicating that some amount of thermal activation for epoxy cross-linking occurs even during photopolymerization alone due to the heat expelled from the light source used. However, this is a minor effect.

The PIGH20 neat and PDMS-containing resins are subjected to DMA characterization, and their results are shown in Figure 7. Figure 7a depicts the storage modulus and tan(δ) curves for various resins. Interestingly, there appears to be no particular trend in cross-link density between these resins as indicated by the rubbery plateau of the storage modulus. This is likely an indication that the behavior in the rubbery plateau is controlled by the network and not by the subdomains. The tan(δ) curves of Figure 7a indicate a slight reduction in the network T_g from ∼78 to ∼74 °C with increasing OH-PDMS content (i.e., with reducing the extent of phase separation), which is also shown in Table 2. This trend is likely due to more PDMS being trapped in the network and acting as a plasticizer rather than being phase separated.

Table 2. Glass Transition Temperatures, T_g, of Both the Network and of the PDMS Subdomains of the PIGH20 Neat and PDMS-Containing Resins Thermally Cured at 165 °C for 48 h, as Obtained from Figure 7. PDMS T_g Values for PIGH20 80:20 and PIGH20 90:10 Represent a Range. Provided Error Represents the Standard Error of the Two Replicates

resin	network glass transition temperature, $T_{g,N}$ (°C)	PDMS glass transition temperature, $T_{g,P}$ (°C)
PIGH20 neat resin	76.9 ± 0.1	
PIGH20 20:80	78.2 ± 0.6	−109.8 ± 0.2
PIGH20 40:60	74.9 ± 0.5	−124.9 ± 0.3
PIGH20 60:40	74.2 ± 0.2	−129.9 ± 1.1
PIGH20 80:20	71.1 ± 2.6	−134.1 ± 1.6 to −115.7 ± 0.6
PIGH20 90:10	74.2 ± 0.5	−137.3 ± 0.3 to −112.0 ± 0.6

The low-temperature segment of the tan(δ) curves in Figure 7a is shown in Figure 7b to visualize the peaks associated with the PDMS subdomains. The PDMS T_g is highest in the case of the largest amount of phase separation (for PIGH20 20:80, the PDMS $T_g \approx -109.8$). In other words, with larger subdomains, larger degrees of cross-linking within the subdomains become possible, even though the stoichiometry of OH-PDMS to epoxy-PDMS becomes more drastically offset. For instance, in the PIGH20 20:80 system, at most 40% of the total PDMS additive may cross-link (20% OH-PDMS, 20% epoxy-PDMS), but cross-linking is more effective due to the larger subdomains that arise from phase separation. On the other hand, as the extent of phase separation decreases, the PDMS T_g shifts to lower temperatures and ultimately the peak becomes a broad shoulder. The presence of this shoulder (e.g., in the PIGH20 80:20 and 90:10 cases, the PDMS T_g is ∼ −134.1 to −115.7 and −137.3 to −112.0 °C respectively) indicates that PDMS is distributed in the network (it is confined by the network) and undergoes different degrees of thermal cross-linking based on the local environment. These results indicate that with smaller subdomains (i.e., more confinement), there will be less cross-linking within the subdomains and a lower PDMS T_g. Table 2 shows the value or range of the PDMS T_g's for the PIGH20 resins tested. The peak in tan(δ) at ∼ −80 °C is a secondary transition of the PIGH20 acrylic network since this peak is present in all systems, including the PIGH20 neat resin.

The mechanical properties of the PIGH20 neat and PDMS-containing resins thermally cured for 48 h at 165 °C are obtained via tensile testing, and the resulting stress−strain curves are shown in Figure 8a. The dashed black line and the black line of the largest peak stress correspond to the PIGH20 neat resin in the states before and after thermal curing, respectively. The respective increase in strength and stiffness of the neat resin after thermal curing is attributed to the predominant cross-linking of epoxy-based chemistries and minor cross-linking of acrylate chemistries as previously confirmed in Figure 6. All PDMS-containing resins have a lower stiffness and strength relative to the thermally cured neat resin. Moreover, the Young's modulus of the various PDMS-containing resins seems to be independent of the OH-PDMS content (Figure 8b), while the peak stress increases with increasing OH-PDMS content as shown in Figure 8c. The elongation at break (Figure 8d) is maximum in the PIGH20 80:20 resin case. The toughness (Figure 8e), determined as the area under the tensile curves of Figure 8a, is largest in the PIGH20 80:20 resin case. We attribute the increase in the ductility in this system to the elastomeric nature of the subdomains. While we cannot probe the mechanical properties of the subdomains directly, we infer from this result that a weakly phase-separated system with lower cross-link density within the subdomains leads to the best ductility and strength combination. Further studies on the mechanical properties of this resin formulation subjected to various thermal curing durations are shown in the Supporting Information (Figure S1).

Since creep is a concern in structural applications, the PIGH20 neat and PIGH20 80:20 resins are subjected to creep resistance testing. Figure 9 shows the variation in time of the creep strain of samples loaded with constant stress equal to 10% of the peak stress of the same material measured in the monotonic uniaxial tension test (Figure 8). Both systems exhibit little creep, with the phase-separating system possessing even better creep resistance than the neat resin when the ratio of the creep stress to the uniaxial peak stress is kept constant. This same trend holds true when samples are subjected to a stress equal to 20% of the peak stress and 35% of the peak stress (Figure 9). This data indicates that the presence of small phase-separated ductile subdomains does not promote creep. When the two materials are instead subjected to the same stress level, it is seen that they creep roughly the same amount as shown in Figure S2 of the Supporting Information.

With all data considered, it is concluded that the PIGH20 80:20 resin formulation produces the desired increase in ductility of the thermosetting network due to the presence of small, loosely cross-linked subdomains. When evaluated at the same stress level, the creep resistance is similar to that of the neat resin, even in the presence of a phase separation.

4. CONCLUSIONS

In this work, photopolymerization-induced phase separation (photo-PIPS) was implemented into a photocurable multi-component monomer resin which possesses both acrylic-based and epoxy-based monomer chemistries (PIGH20 neat resin).

https://doi.org/10.1021/acsapm.3c03155
ACS Appl. Polym. Mater. 2024, 6, 5028−5038

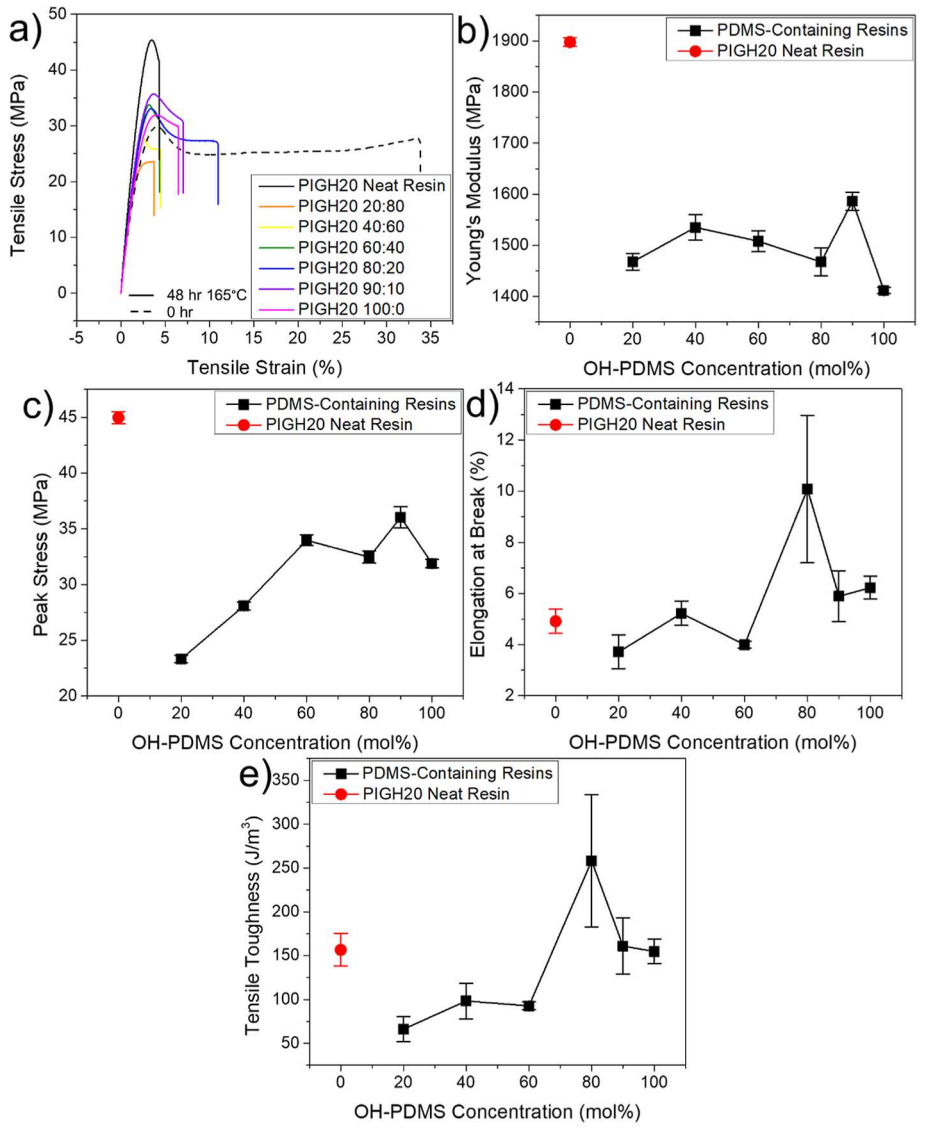

Figure 8. (a) Tensile nominal stress−strain curves for the PIGH20 neat and PDMS-containing resins thermally cured for 48 h at 165 °C. The dashed line shows the stress−strain curve for the PIGH20 neat resin before thermal curing. (b) Corresponding Young's modulus, (c) peak stress, (d) elongation at break, and (e) toughness (area under the tensile curve) of the PDMS-containing resins plotted versus OH-PDMS concentration. The respective mechanical property values of the PIGH20 neat resin thermally cured for 48 h at 165 °C are also represented in plots (b−e). Error bars represent the standard error out of four replicates per sample.

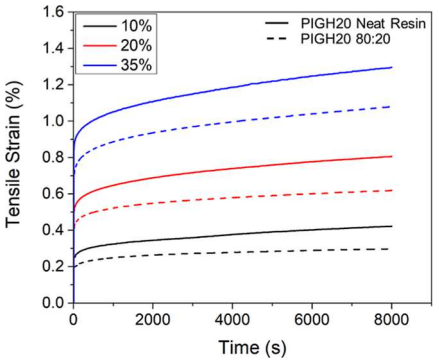

Figure 9. Creep strain versus time curves determined for the PIGH20 neat and PIGH20 80:20 resins thermally cured at 165 °C for 48 h. Several constant applied stresses of 10, 20, and 35% of the peak stress of each resin are used.

Photopolymerization develops the network by reaction of the acrylic monomers, while subsequent thermal curing produces increased strength and stiffness of the network by cross-linking between the epoxy-based monomers. Phase separation was created by the addition of two PDMS-based polymer additives to the PIGH20 neat resin, one with alcohol and the other with epoxide end groups, which form PDMS-rich subdomains during network photopolymerization. The two PDMS components react during the thermal curing step, rendering the phase-separated subdomains elastomeric.

The extent of phase separation depends on the relative concentration of the epoxy-PDMS and OH-PDMS, with OH-PDMS present alone being nonphase-separating. Systems with multiple relative concentrations of the two moieties were considered, and it was observed that the strength increases with increasing the concentration of OH-PDMS, the stiffness is approximately insensitive to this parameter, and the ductility is maximum in the PIGH20 80:20 system. This system has small

https://doi.org/10.1021/acsapm.3c03155
ACS Appl. Polym. Mater. 2024, 6, 5028−5038

subdomains, and the degree of cross-linking within the subdomains is likely low, which suggests that soft, deformable, and small (micrometer and below) subdomains well bonded to the surrounding network improve the toughness of the photocurable thermoset. Furthermore, by altering the chemistries of the phase-separated material, different applications can be feasible, including polymer membrane technologies, polymer composites, and even polymer-dispersed liquid crystal applications.

■ ASSOCIATED CONTENT

Supporting Information

The Supporting Information is available free of charge at https://pubs.acs.org/doi/10.1021/acsapm.3c03155.

Tensile testing and creep resistance of PIGH20 neat and 80:20 resins (PDF)

■ AUTHOR INFORMATION

Corresponding Author

Catalin R. Picu − *Department of Mechanical, Aerospace and Nuclear Engineering, Rensselaer Polytechnic Institute, Troy, New York 12180, United States;* orcid.org/0000-0001-8371-3564; Phone: 1 518 276 2195; Email: picuc@rpi.edu

Authors

Lauren Zakrzewski − *Department of Chemistry and Chemical Biology, Rensselaer Polytechnic Institute, Troy, New York 12180, United States*

Kanta Das Purkaysta − *Department of Mechanical, Aerospace and Nuclear Engineering, Rensselaer Polytechnic Institute, Troy, New York 12180, United States*

Chulsung Bae − *Department of Chemistry and Chemical Biology, Rensselaer Polytechnic Institute, Troy, New York 12180, United States;* orcid.org/0000-0002-9026-3319

Complete contact information is available at: https://pubs.acs.org/10.1021/acsapm.3c03155

Notes

The authors declare no competing financial interest.

■ ACKNOWLEDGMENTS

This research was supported by the NSF through grant CMMI-2007909 and Korea Evaluation Institute of Industrial Technology through Development of Core Industrial Technology (Project no. 20000965), funded by the Ministry of Trade, Industry & Energy of Korea.

■ REFERENCES

(1) Park, S.; Kim, H. K.; Hong, J. W. Investigation of the Photopolymerization-Induced Phase Separation Process in Polymer Dispersed Liquid Crystal. *Polym. Test.* **2010**, *29* (7), 886−893.

(2) Smith, D. M.; Li, C. Y.; Bunning, T. J. Light-Directed Mesoscale Phase Separation via Holographic Polymerization. *J. Polym. Sci. B Polym. Phys.* **2014**, *52* (3), 232−250.

(3) Hu, Y.-X.; Hao, X.; Xu, L.; Xie, X.; Xiong, B.; Hu, Z.; Sun, H.; Yin, G.-Q.; Li, X.; Peng, H.; Yang, H.-B. Construction of Supramolecular Liquid-Crystalline Metallacycles for Holographic Storage of Colored Images. *J. Am. Chem. Soc.* **2020**, *142* (13), 6285−6294.

(4) Zhao, Y.; Peng, H.; Zhou, X.; Li, Z.; Xie, X. Interfacial AIE for Orthogonal Integration of Holographic and Fluorescent Dual-Thermosensitive Images. *Adv. Sci.* **2022**, *9* (10), 2105903.

(5) Wei, W.; Chen, G.; Li, S.; Zhou, X.; Peng, H.; Xie, X.; Mai, Y.-W. Computational Insight into Phase Separation of a Thiol-Ene Photopolymer with Liquid Crystals for Holography by Dissipative Particle Dynamics Simulation. *Macromolecules* **2023**, *56* (14), 5457−5469.

(6) Roh, I. J.; Ramaswamy, S.; Krantz, W. B.; Greenberg, A. R. Poly(Ethylene Chlorotrifluoroethylene) Membrane Formation via Thermally Induced Phase Separation (TIPS). *J. Membr. Sci.* **2010**, *362* (1−2), 211−220.

(7) Schulze, M. W.; McIntosh, L. D.; Hillmyer, M. A.; Lodge, T. P. High-Modulus, High-Conductivity Nanostructured Polymer Electrolyte Membranes via Polymerization-Induced Phase Separation. *Nano Lett.* **2014**, *14* (1), 122−126.

(8) Chopade, S. A.; Au, J. G.; Li, Z.; Schmidt, P. W.; Hillmyer, M. A.; Lodge, T. P. Robust Polymer Electrolyte Membranes with High Ambient-Temperature Lithium-Ion Conductivity via Polymerization-Induced Microphase Separation. *ACS Appl. Mater. Interfaces* **2017**, *9* (17), 14561−14565.

(9) Radu, E. R.; Voicu, S. I.; Thakur, V. K. Polymeric Membranes for Biomedical Applications. *Polymers (Basel)* **2023**, *15* (3), 619.

(10) Torbati, A. H.; Nejad, H. B.; Ponce, M.; Sutton, J. P.; Mather, P. T. Properties of Triple Shape Memory Composites Prepared via Polymerization-Induced Phase Separation. *Soft Matter* **2014**, *10* (17), 3112−3121.

(11) Zhang, P.; Sundberg, D. C.; Tsavalas, J. G. Polymerization Induced Phase Separation in Composite Latex Particles during Seeded Emulsion Polymerization. *Ind. Eng. Chem. Res.* **2019**, *58*, 21118−21129.

(12) Zhang, P.; Gao, Z.; Zhang, Q.; Khattab, A.; Li, G. Fracture Behavior Characterization of Arcan Polycaprolactone Based Polymer Composites Prepared by Polymerization Induced Phases Separation. *Polym. Compos.* **2019**, *40* (3), 1198−1208.

(13) Anastasio, R.; Peerbooms, W.; Cardinaels, R.; Van Breemen, L. C. A. Characterization of Ultraviolet-Cured Methacrylate Networks: From Photopolymerization to Ultimate Mechanical Properties. *Macromolecules* **2019**, *52* (23), 9220−9231.

(14) Ligon, S. C.; Liska, R.; Stampfl, J.; Gurr, M.; Mülhaupt, R. Polymers for 3D Printing and Customized Additive Manufacturing. *Chem. Rev.* **2017**, *117* (15), 10212−10290.

(15) Hofmann, M. 3D Printing Gets a Boost and Opportunities with Polymer Materials. *ACS Macro Lett.* **2014**, *3* (4), 382−386.

(16) Bonnet, A.; Pascault, J. P.; Sautereau, H.; Taha, M.; Camberlin, Y. Epoxy-Diamine Thermoset/Thermoplastic Blends. 1. Rates of Reactions before and after Phase Separation. *Macromolecules* **1999**, *32* (25), 8517−8523.

(17) Willemse, R. C.; Ramaker, E. J. J.; Van Dam, J.; Posthuma De Boer, A. Morphology Development in Immiscible Polymer Blends: Initial Blend Morphology and Phase Dimensions. *Polymer (Guildf)* **1999**, *40*, 6651−6659.

(18) Veenstra, H.; Van Dam, J.; Posthuma De Boer, A. On the Coarsening of Co-Continuous Morphologies in Polymer Blends: Effect of Interfacial Tension, Viscosity and Physical Cross-Links. *Polymer (Guildf)* **2000**, *41*, 3037−3045.

(19) Murata, K.; Sachin, J.; Etori, H.; Anazawa, T. Photopolymerization-Induced Phase Separation in Binary Blends of Photocurable/Linear Polymers. *Polymer (Guildf)* **2002**, *43*, 2845−2859.

(20) Sasaki, Y.; Aiba, N.; Hashimoto, H.; Kumaki, J. Reversible Hierarchical Phase Separation of a Poly(Methyl Methacrylate) and Poly(n -Nonyl Acrylate) Blend in a Langmuir Monolayer. *Macromolecules* **2010**, *43* (21), 9077−9086.

(21) Naderi, N.; Rastegar, S.; Mohseni, M.; Khorasani, M. Photo-Polymerization Induced Viscoelastic Phase Separation of Trimethylolpropane Triacrylate/Poly (Styrene-Co-Methyl Methacrylate) Blends. *Polymer (Guildf)* **2018**, *153*, 391−397.

(22) Naderi, N.; Rastegar, S.; Mohseni, M.; Khorasani, M. Controlling Final Morphologies of Two-Step Polymerization Induced Phase Separated Blends of Trimethylolpropane Triacrylate/Acrylate

Copolymer through Copolymer Molecular Weight. *Polym. Test.* **2017**, *61*, 146−149.
(23) Lipic, P. M.; Bates, F. S.; Hillmyer, M. A. Nanostructured Thermosets from Self-Assembled Amphiphilic Block Copolymer/Epoxy Resin Mixtures. *J. Am. Chem. Soc.* **1998**, *120*, 8963−8970.
(24) Lodge, T. P. Block Copolymers: Past Successes and Future Challenges. *Macromol. Chem. Phys.* **2003**, *204* (2), 265−273.
(25) Clapper, J. D.; Skeie, J. M.; Mullins, R. F.; Guymon, C. A. Development and Characterization of Photopolymerizable Biodegradable Materials from PEG-PLA-PEG Block Macromonomers. *Polymer (Guildf)* **2007**, *48* (22), 6554−6564.
(26) Mai, Y.; Eisenberg, A. Self-Assembly of Block Copolymers. *Chem. Soc. Rev.* **2012**, *41* (18), 5969−5985.
(27) Lu, J.; Wool, R. P. Additive Toughening Effects on New Bio-Based Thermosetting Resins from Plant Oils. *Compos. Sci. Technol.* **2008**, *68*, 1025−1033.
(28) Hayes, B. S.; Seferis, J. C. Modification of Thermosetting Resins and Composites through Preformed Polymer Particles: A Review. *Polym. Compos.* **2001**, *22* (4), 451−467.
(29) Liu, K.; Macosko, C. W. Can Nanoparticle Toughen Fiber-Reinforced Thermosetting Polymers? *J. Mater. Sci.* **2019**, *54*, 4471−4483.
(30) Huang, Y.; Hunston, D. L.; Kinloch, A. J.; Riew, C. K. Mechanisms of Toughening Thermoset Resins. *Adv. Chem.* **1993**, *233*, 1−35.
(31) Williams, R. J. J.; Rozenberg, B. A.; Pascault, J.-P. Reaction-Induced Phase Separation in Modified Thermosetting Polymers. *Adv. Polym. Sci.* **1997**, *128*, 95−156.
(32) Bian, X.; Tuo, R.; Yang, W.; Zhang, Y.; Xie, Q.; Zha, J.; Lin, J.; He, S. Mechanical, Thermal, and Electrical Properties of BN-Epoxy Composites Modified with Carboxyl-Terminated Butadiene Nitrile Liquid Rubber. *Polymers (Basel)* **2019**, *11* (10), 1548.
(33) Ligon-Auer, S. C.; Schwentenwein, M.; Gorsche, C.; Stampfl, J.; Liska, R. Toughening of Photo-Curable Polymer Networks: A Review. *Polym. Chem.* **2016**, *7* (2), 257−286.
(34) Parameswaranpillai, J.; Hameed, N.; Pionteck, J.; Woo, E. M. *Handbook of Epoxy Blends*; Springer International Publishing, 2016..
(35) Hsieh, T. H.; Kinloch, A. J.; Taylor, A. C.; Sprenger, S. The Effect of Silica Nanoparticles and Carbon Nanotubes on the Toughness of a Thermosetting Epoxy Polymer. *J. Appl. Polym. Sci.* **2011**, *119* (4), 2135−2142.
(36) Tang, Y.; Ye, L.; Zhang, Z.; Friedrich, K. Interlaminar Fracture Toughness and CAI Strength of Fibre-Reinforced Composites with Nanoparticles - A Review. *Compos. Sci. Technol.* **2013**, *86*, 26−37.
(37) Alam, T. M.; Ahn, J.; Lee, S.; Leguizamon, S. C.; Jones, B. H. Dynamic Heterogeneity and Nanophase Separation in Rubber-Toughened Amine-Cured Highly Cross-Linked Polymer Networks. *Polym. Test.* **2022**, *112*, 107616.
(38) Seo, M.; Hillmyer, M. A. Reticulated Nanoporous Polymers by Controlled Polymerization-Induced Microphase Separation. *Science (1979)* **2012**, *336* (6087), 1422−1425.
(39) Williams, R. J. J.; Hoppe, C. E.; Zucchi, I. A.; Romeo, H. E.; dell'Erba, I. E.; Gómez, M. L.; Puig, J.; Leonardi, A. B. Self-Assembly of Nanoparticles Employing Polymerization-Induced Phase Separation. *J. Colloid Interface Sci.* **2014**, *431*, 223−232.
(40) Szczepanski, C. R.; Stansbury, J. W. Modification of Linear Prepolymers to Tailor Heterogeneous Network Formation through Photo-Initiated Polymerization-Induced Phase Separation. *Polymer (Guildf)* **2015**, *70*, 8−18.
(41) Boots, H. M. J.; Kloosterboer, J. G.; Serbutoviez, C.; Touwslager, F. J. Polymerization-Induced Phase Separation. 1. Conversion-Phase Diagrams. *Macromolecules* **1996**, *29*, 7683−7689.
(42) Serbutoviez, C.; Kloosterboer, J. G.; Boots, H. M. J.; Touwslager, F. J. Polymerization-Induced Phase Separation. 2. Morphology of Polymer-Dispersed Liquid Crystal Thin Films. *Macromolecules* **1996**, *29*, 7690−7698.
(43) Szczepanski, C. R.; Stansbury, J. W. Accessing Photo-Based Morphological Control in Phase-Separated, Cross-Linked Networks through Delayed Gelation. *Eur. Polym. J.* **2015**, *67*, 314−325.
(44) Yamashita, Y.; Komori, K.; Murata, T.; Nakanishi, H.; Norisuye, T.; Yamao, T.; Tran-Cong-Miyata, Q. Conducting Polymer Networks Synthesized by Photopolymerization-Induced Phase Separation. *Adv. Nat. Sci.: Nanosci. Nanotechnol.* **2018**, *9* (1), 015009.
(45) Zakrzewski, L.; Ryu, C. Y.; Bae, C.; Picu, C. R. Photopolymerization-Induced Phase Separation Kinetics Explored by Intermittent Irradiation. *Polymer (Guildf)* **2024**, *290*, 126526.
(46) Zakrzewski, L.; Kim, Y.; Song, Y.; Ryu, C. Y.; Bae, C.; Picu, C. R. Interplay of Photopolymerization and Phase Separation Kinetics and the Resulting Structure-Property Relationship of Photocurable Resins. *Polymer (Guildf)* **2023**, *280*, 126032.
(47) Hara, A.; Inoue, R.; Takahashi, N.; Nishida, K.; Kanaya, T. Trajectory of Critical Point in Polymerization-Induced Phase Separation of Epoxy/Oligoethylene Glycol Solutions. *Macromolecules* **2014**, *47* (13), 4453−4459.
(48) Tang, Y.; Wu, K.; Yu, S.; Chen, J.; Ding, X.; Rao, L.; Li, Z. Bioinspired High-Scattering Polymer Films Fabricated by Polymerization-Induced Phase Separation. *Opt. Lett.* **2020**, *45* (10), 2918−2921.
(49) Wang, F.; Ratke, L.; Zhang, H.; Altschuh, P.; Nestler, B. A Phase-Field Study on Polymerization-Induced Phase Separation Occasioned by Diffusion and Capillary Flow—a Mechanism for the Formation of Porous Microstructures in Membranes. *J. Solgel Sci. Technol.* **2020**, *94* (2), 356−374.
(50) Kahrs, C.; Gühlstorf, T.; Schwellenbach, J. Influences of Different Preparation Variables on Polymeric Membrane Formation via Nonsolvent Induced Phase Separation. *J. Appl. Polym. Sci.* **2020**, *137* (28), 48852.
(51) Abouhamzeh, M.; Sinke, J.; Benedictus, R. Prediction Models for Distortions and Residual Stresses in Thermoset Polymer Laminates: An Overview. *J. Manuf. Mater. Process.* **2019**, *3* (4), 87.
(52) Abe, A.; Albertsson, A. C.; Cantow, H. J.; Dusek, K.; Edwards, S.; Hocker, H.; Joanny, J. F.; Kausch, H. H.; Lee, K. S.; McGrath, J. E.; Monnerie, L.; Stupp, S. I.; Suter, U. W.; Wegner, G.; Young, R. J. *Advances in Polymer Science: Molecular Simulation Fracture Gel Theory*; Springer-Verlag, 2002; Vol. *156*.
(53) Auschra, C.; Stadler', R. Polymer alloys based on poly(2,6-dimethyl-1,4-phenylene ether) and poly(styrene-co-acrylonitrile) using poly(styrene-b-(ethylene-co-butylene)-b-methyl methacrylate) triblock copolymers as compatibilizers. *Macromolecules* **1993**, *26*, 6364−6377.
(54) Wilson-Heid, A. E.; Beese, A. M. Combined Effects of Porosity and Stress State on the Failure Behavior of Laser Powder Bed Fusion Stainless Steel 316L. *Addit. Manuf.* **2021**, *39*, 101862.
(55) Charton, C.; Falk, V.; Marchal, P.; Pla, F.; Colon, P. Influence of Tg, Viscosity and Chemical Structure of Monomers on Shrinkage Stress in Light-Cured Dimethacrylate-Based Dental Resins. *Dent. Mater.* **2007**, *23* (11), 1447−1459.
(56) Prasatya, P.; McKenna, G. B.; Simon, S. L. A Viscoelastic Model for Predicting Isotropic Residual Stresses in Thermosetting Materials: Effects of Processing Parameters. *J. Compos. Mater.* **2001**, *35* (10), 826−848.
(57) Chartoff, R. P.; Flach, L.; Weissman, P. *Material and Process Parameters that Affect Accuracy in Stereolithography*: Dayton, OH, 1993.
(58) Al Sunbul, H.; Silikas, N.; Watts, D. C. Polymerization Shrinkage Kinetics and Shrinkage-Stress in Dental Resin-Composites. *Dent. Mater.* **2016**, *32* (8), 998−1006.
(59) Ellakwa, A.; Cho, N.; Lee, I. B. The Effect of Resin Matrix Composition on the Polymerization Shrinkage and Rheological Properties of Experimental Dental Composites. *Dent. Mater.* **2007**, *23* (10), 1229−1235.
(60) Karalekas, D.; Rapti, D.; Gdoutos, E. E.; Aggelopoulos, A. Investigation of Shrinkage-Induced Stresses in Stereolithography Photo-Curable Resins. *Exp. Mech.* **2002**, *42* (4), 439−444.
(61) Dewaele, M.; Truffier-Boutry, D.; Devaux, J.; Leloup, G. Volume Contraction in Photocured Dental Resins: The Shrinkage-Conversion Relationship Revisited. *Dent. Mater.* **2006**, *22* (4), 359−365.

https://doi.org/10.1021/acsapm.3c03155
ACS Appl. Polym. Mater. 2024, 6, 5028−5038

(62) Kimura, N.; Kawazoe, K.; Nakanishi, H.; Norisuye, T.; Tran-Cong-Miyata, Q. Influences of Wetting and Shrinkage on the Phase Separation Process of Polymer Mixtures Induced by Photopolymerization. *Soft Matter* **2013**, *9* (35), 8428−8437.
(63) Andrzejewska, E. Photopolymerization Kinetics of Multifunctional Monomers. *Prog. Polym. Sci.* **2001**, *26*, 605−665.
(64) Beuermann, S.; Buback, M. Rate Coefficients of Free-Radical Polymerization Deduced from Pulsed Laser Experiments. *Prog. Polym. Sci.* **2002**, *27*, 191−254.
(65) Kilambi, H.; Stansbury, J. W.; Bowman, C. N. Enhanced Reactivity of Monovinyl Acrylates Characterized by Secondary Functionalities toward Photopolymerization and Michael Addition: Contribution of Intramolecular Effects. *J. Polym. Sci. A Polym. Chem.* **2008**, *46* (10), 3452−3458.
(66) McCoy, J. D.; Ancipink, W. B.; Clarkson, C. M.; Kropka, J. M.; Celina, M. C.; Giron, N. H.; Hailesilassie, L.; Fredj, N. Cure Mechanisms of Diglycidyl Ether of Bisphenol A (DGEBA) Epoxy with Diethanolamine. *Polymer (Guildf)* **2016**, *105*, 243−254.
(67) Shechter, L.; Wynstra, J. Glycidyl Ether Reactions with Alcohols, Phenols, Carboxylic Acids, and Acid Anhydrides. *Ind. Eng. Chem.* **1956**, *48* (1), 86−93.
(68) Young, R. J.; Lovell, P. A. *Introduction to Polymers*, 3rd ed.; CRC Press, 2011.
(69) Kim, Y.; Song, Y.; Ryu, C. Y.; Bae, C.; Picu, C. R. Reactive UV Transmittance Analysis in Photopolymerization Induced Phase Separation. Manuscript in Preparation **2024**.
(70) Beyerer, J.; Puente León, F.; Frese, C. *Machine Vision Automated Visual Inspection: Theory, Practice and Applications*, 1st ed.; Springer-Verlag, 2016. .

https://doi.org/10.1021/acsapm.3c03155
ACS Appl. Polym. Mater. 2024, 6, 5028−5038